Geoeffectiveness of corotating interaction regions as measured by *Dst* index

M. V. Alves,[1] E. Echer,[2] and W. D. Gonzalez[2]

Received 23 August 2005; revised 23 October 2005; accepted 28 November 2005; published 12 May 2006.

[1] Corotating interaction regions (CIRs) are structures formed when high-speed solar wind streams overtake slow solar wind streams as they propagate outward. These structures produce regions of enhanced density and magnetic field strength in the solar wind near the ecliptic plane. In this paper, the geoeffectiveness of CIRs, as measured by the geomagnetic *Dst* index, is assessed during the solar wind observational period 1964–2003. A catalogue of CIRs is constructed by consulting high-speed plasma streams (HSPS) lists present in the literature and by analyzing solar wind parameters for each HSPS event. The geoeffectiveness of CIRs is analyzed by determining the number of intense ($Dst \leq -100$ nT), moderate ($-100 < Dst \leq -50$ nT), or weak ($-50 < Dst \leq -30$ nT) magnetic storms that followed each CIR event. Statistical distributions of CIR parameters (maximum solar wind speed, maximum convection electric field, southward magnetic field peak) and geoeffectiveness (*Dst* peak) are obtained. Correlation analyses of *Dst* index with various solar wind parameters are presented. A comparison with the geoeffectiveness of other interplanetary structures such as shocks, magnetic clouds, and sector boundaries is performed. Our results show that 33% of CIRs are followed by moderate/intense magnetic activity ($Dst < -50$ nT), i.e., approximately one third of the CIR events observed near Earth are geoeffective.

Citation: Alves, M. V., E. Echer, and W. D. Gonzalez (2006), Geoeffectiveness of corotating interaction regions as measured by *Dst* index, *J. Geophys. Res.*, *111*, A07S05, doi:10.1029/2005JA011379.

1. Introduction

[2] The geoeffectiveness, i.e., the ability to significantly disturb the geospace, of various solar and interplanetary phenomena such as interplanetary shocks, ejected plasma clouds from solar flares/coronal mass ejections (CMEs), corotating high-speed streams from coronal holes, and interaction region/stream interfaces, have been of considerable interest to solar terrestrial physics community [*Gosling et al.*, 1990; *Gonzalez et al.*, 1999; *Yermolaev et al.*, 2005]. Interplanetary remnants of CMEs (ICMEs) and corotating interaction regions (CIRs) have been thought to be the two major interplanetary sources of geomagnetic disturbances. Interplanetary manifestations of fast coronal mass ejections are the dominant interplanetary phenomena causing magnetic storms around solar maximum. During solar minimum, CIRs play a dominant role as a source of geomagnetic disturbances [*Gonzalez et al.*, 1999; *Tsurutani et al.*, 1995]. Looking for sources of geomagnetic activity during the period 1972–1986, *Richardson et al.* [2000] found that during solar minimum, the Earth was embedded in corotating streams for 60% of the time versus 30% for slow solar wind and $<\sim$10% for CMEs. They also found that at solar maximum, corotating streams, slow solar wind, and CME-related structures were each present for around one-third of the time.

[3] Fast streams, with speed exceeding 700 km/s, are originated in the coronal holes, as confirmed by Ulysses observations [*Phillips et al.*, 1994]. Coronal holes are regions in the Sun with abnormally low density, where magnetic field has a single polarity, all inward or outward (open lines). This open magnetic field goes out to interplanetary space, rapidly diverging. A coronal hole emits less light at all wavelengths than surrounding regions, and it appears in X-ray images as a black area [*Krieger et al.*, 1973; *Timothy et al.*, 1975]. In general, less than 20% of the solar surface is composed of coronal holes, localized close to polar region. During the declining phase of the $\sim$11-year solar activity cycles the coronal holes are largest and they can extend to latitudes close to the ecliptic plane [*Sheeley and Harvey*, 1981; *Jackson*, 1997; *Burlaga et al.*, 1978]. During this phase, as the Sun rotates, fast wind follows slow wind, and as the streams propagate away from the Sun, the fast wind catches up with the slow wind, compressing the plasma at the boundary, increasing the density in the slow solar wind region. In the fast solar wind the kinetic energy of the plasma is converted into thermal energy, resulting in plasma heating and density decreasing (rarefaction). This contact between the slow and fast solar wind is called the stream interface (SI). If the configuration of the solar corona is stable, the pattern of interaction regions is repeated each time the Sun rotates, and they are called corotating interaction regions (CIRs) [*Smith and Wolf*, 1976].

[1]Laboratório Associado de Plasma, Instituto Nacional de Pesquisas Espaciais, São José dos Campos, São Paulo, Brazil.
[2]Divisão de Geofísica Espacial, Instituto Nacional de Pesquisas Espaciais, São José dos Campos, São Paulo, Brazil.

0148-0227/06/2005JA011379

[4] During the descending phase of the solar cycle, high-velocity solar ejecta occur less frequently, and corotating high-speed streams occur more often [*Feynman and Gu*, 1986]. An illustration of the formation of a CIR in presented in Figure 1 (from *Pizzo* [1978]). We notice that the magnetic field lines of the ambient solar wind are more curved, whereas those of the high-speed streams are more radial. The compression and rarefaction zones might be preceded by a fast and reverse MHD shocks, respectively, especially beyond ~2 AU. At 1 AU, CIRs are not as well-developed as they are at greater heliocentric distances. The reverse waves sometimes steepen into shocks by 1 AU, while the forward waves rarely do so [*Kamide et al.*, 1998]. They further tend to have rapidly fluctuating and small enhancements of the southward component of the interplanetary magnetic field (B_s). Within the stream the magnetic field maintains the same polarity, which is the same as in the corresponding coronal hole.

[5] The fast streams are the main cause of recurring geomagnetic storms [*Hargreaves*, 1992; *Hundhausen*, 1995; *Gosling and Pizzo*, 1999]. *Crooker and Cliver* [1994] reemphasized the importance of the association between recurrent storms and CIRs. At the same time they raised the possibility that CMEs may play a central role in recurrent as well as nonrecurrent storms. *Gosling and Pizzo* [1999] presented an overview of observations as well as numerical models that describe the physical origin and radial evolution of CIRs. Correlated to the last-mentioned paper, *Forsyth and Marsch* [1999] presented some important facts and open questions about the origin and nature of the boundary between fast and slow solar wind near the Sun, the evolution of stream interfaces with heliocentric distance in the inner heliosphere, and their relationship. It is the increasing interaction between these fast and slow flows with distance from the Sun that leads to the establishment of CIRs.

[6] The response of geomagnetic activity to the interaction regions described above has been studied by many workers [*Burlaga and Lepping*, 1977; *Tsurutani et al.*, 1995; *Lindsay et al.*, 1995; *Badruddin*, 1998, and references therein]. Significant geomagnetic changes have been associated to the transit of interaction regions and different reasons for that have been suggested. It has been understood for some time that solar wind (SW) disturbances lead to magnetic storms and that they have their greatest effects when the disturbance has a combination of large plasma velocities (V_{sw}) and large southward component of the interplanetary magnetic field (B_s) [*Gonzalez and Tsurutani*, 1987; *Gonzalez et al.*, 1994], i.e., is the dawn-dusk electric field (Ey) that drives magnetospheric convection. Magnetic reconnection is the mechanism that allows the solar wind energy entrance in the magnetosphere [*Dungey*, 1961]. Slow solar wind usually does not contain long intervals of a significant B_s. However, large-scale disturbances propagate in the SW carrying or driving large B_s. As far as geomagnetic activity is concerned, the most important feature of CIRs is that they are characterized by intense magnetic fields. While the typical value of the IMF intensity is about 10–15 nT within CIRs, for some of them the IMF intensity can reach ≈30 nT [*Gonzalez et al.*, 1999].

[7] The geomagnetic activity has a very well-known semiannual variation, with peaks around equinoxes, attributed to the Russell-McPherron effect [*Russell and McPherron*, 1973]. The Russell-McPherron effect is based on the simple geometric mapping from the solar equatorial (GSE) plane, in which the prevailing IMF is ordered, into a magnetospheric system (GSM) which orders the response. The result of the offsets between the solar equatorial, ecliptic, and terrestrial rotational planes is to create a seasonal modulation in the rotation from the transverse solar equatorial IMF component (GSE B_y) into north-south field in the magnetospheric system (GSM B_z). The tilt of the terrestrial dipole adds a diurnal component. As a result, the toward sector, negative B_y, is more effective on April equinox, while the away sector, positive B_y, is more effective on September equinox. *Crooker and Cliver* [1994] demonstrated that the Russell-McPherron effect exerts strong control over recurrent activity. CIRs enhance the Russell-McPherron effect by increasing the magnitude of the predominantly ecliptic fields there, thereby increasing the projected southward component of the resulting peak recurrent activity.

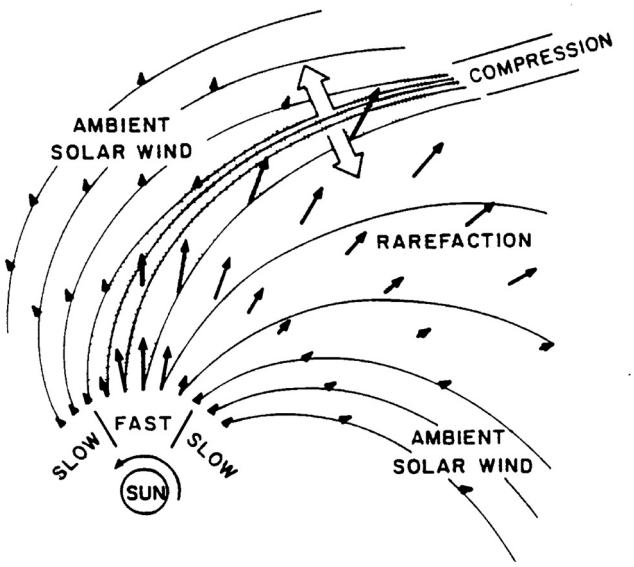

Figure 1. Schematic illustration of a fast stream interacting with a slow stream (from *Pizzo* [1978]).

[8] In this paper we analyzed the geoeffectiveness of 727 CIR events, registered from 1964 to 2003. We use measurements of the *Dst* index as an indicator of the geomagnetic activity. The *Dst* index is basically derived from the H-component measured by ground-based low-latitude geomagnetic observatories. The magnitude of *Dst* is proportional to the kinetic energy of ring current particles. It describes well the development of global large-scale geomagnetic disturbances (magnetic storms) [*Gonzalez et al.*, 1994]. For each CIR event we found the minimum value of *Dst* index, within 2 days following the data of the observation of the SI region. A statistical analysis of these events is performed, investigating the geoeffectiveness of them. We have also investigated the distribution of percentage of CIRs against maximum/minimum solar wind parameters: solar wind speed (V_{sw}), magnitude of magnetic field (B), southward component of B (B_s), and convection electric field ($Ey = -V_{sw}B_s$). Correlation analyses of *Dst* index with solar

wind parameters (V_{sw}, B_s, and Ey) are presented. Concerning *Dst* values, our results show that only approximately 3% of CIRs are associated with intense storms ($-100 \leq$ *Dst*); if we consider the range of *Dst* < −50 nT (intense + moderate activity), our results show that 33% of CIRs are geoeffective. When we analyze the geomagnetic storms occurred during equinox period, we found that approximately 50% of the CIR events are associated with intense/moderate storms, reflecting the Russell-McPherron effect. As a general result, we could say that CIRs are less geoeffective than transient disturbances (shocks and MCs), although they are followed by a higher number of intense or moderate storms than heliospheric current sheet (HCS) sector boundary crossing events.

2. Selection of Events

[9] The CIR events used here were selected by consulting high-speed plasma streams (HSPS) catalogues found in the literature within the period 1964–2003 [*Lindblad and Lundstedt*, 1981; *Lindblad and Lundstedt*, 1983; *Lindblad et al.*, 1989; *Mavromichalaki et al.*, 1988; *Mavromichalaki and Vassilaki*, 1998]. It is important to mention that although these catalogues include all high-speed plasma streams observed in the solar wind, we selected only the ones classified as CIR. Besides these catalogues we also used lists compiled by R. L. McPherron (1994–1996) and by I. G. Richardson (1994–2003) (I. G. Richardson, personal communication, 2004). The basic physical features of the corotating high-speed streams with respect to interplanetary plasma and field parameters can be summarized as follows: The proton density (n) rises to unusually high values near the leading edges of the streams; the high densities generally persisted for ~1 day. The density profile generally seems to be developed in the inverse ratio to the bulk speed (V_{sw}). The peak of the interplanetary magnetic field in the stream-front compression is proportional to bulk speed with a constant polarity throughout the stream except for some fluctuations lasting a few hours [*Iucci et al.*, 1979; *Tsurutani et al.*, 1987]. The proton temperature (T) varies in a pattern similar to that of the flow velocity. It increases with speed and shows a slight decrease during the magnetic field descent phase [*Mavromichalaki and Vassilaki*, 1998].

[10] We checked each event in the lists to see if they were not interplanetary remnants of coronal mass ejection (ICMEs). This was done using other author catalogs of shocks and ICMEs [*Cane and Richardson*, 2003; *Echer et al.*, 2005a, and references therein]. This analysis was further done by checking the plasma beta parameter (β). This cross-checking and also the analysis of solar wind parameters, n, T, and B, have permitted us to identify the interaction regions between the slow and fast solar wind streams. Events associated with flares, with ICMEs, with magnetic clouds (MCs), and with shocks were not included. Here we have also excluded storms that were caused by the interaction of MCs or shocks with CIRs, i.e., the case when the B_s causing the storm was not only the CIR field but an altered field due to the interaction with a different magnetic structure. We classified each event according to solar wind data quality, defining a Q parameter as follows: (1) if all three parameters, n, V_{sw}, and B are continuous; (2) if the three parameters, n, V_{sw}, and B are present with some short gaps (few hours) or only two parameters are continuous; (3) if only one parameter is continuous or at least one of the parameters presents large gaps (≥1/2 day); if the gap in solar wind data is too large (>1 day), that events were not used. Using the above criteria, a total of 727 CIRs were selected as with enough data to permit further study.

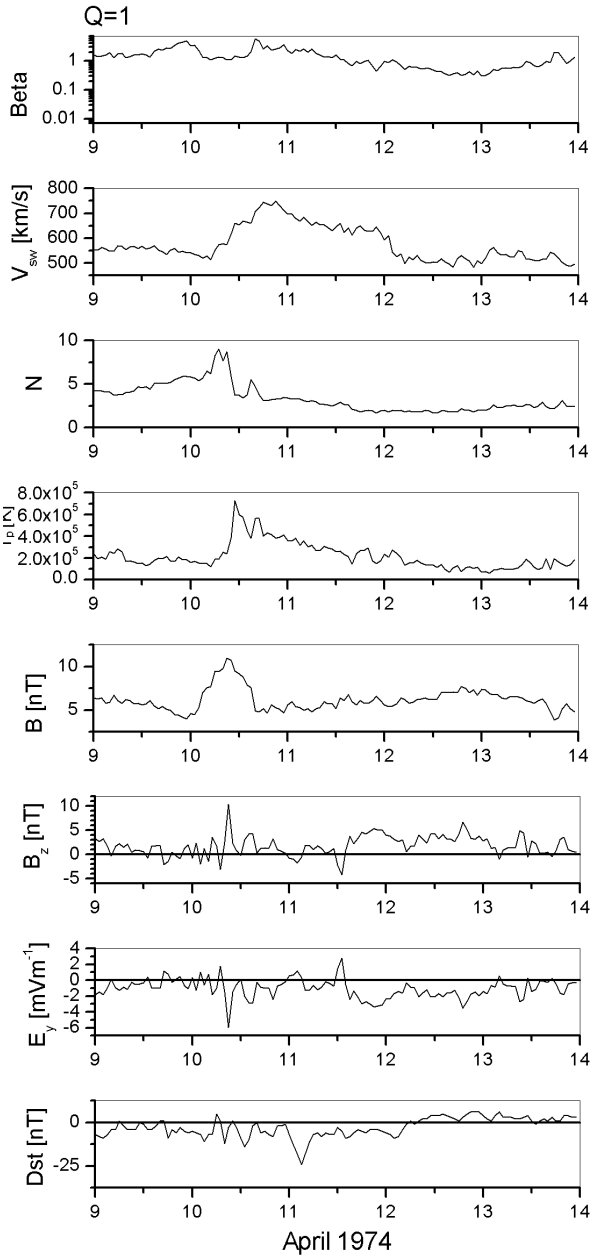

Figure 2. Example of event according quality of data, Q = 1. Plots are, from top to bottom, time variations of plasma parameters β, V_{sw}, n, T, B, B_s, E_y, and *Dst* index.

[11] As an example of the data we used, we present in Figure 2, an event with data quality Q = 1. Figures 3 and 4 present events with data quality 2 and 3, respectively. Figures 2–4 show, from top to bottom, time variations of plasma parameters β, V_{sw}, n, T, B, B_s, E_y, and *Dst* index.

[12] For all CIR events, we examined near-Earth solar wind data from the National Space Science Data Center OMNI database. Solar wind data after 1995 were analyzed

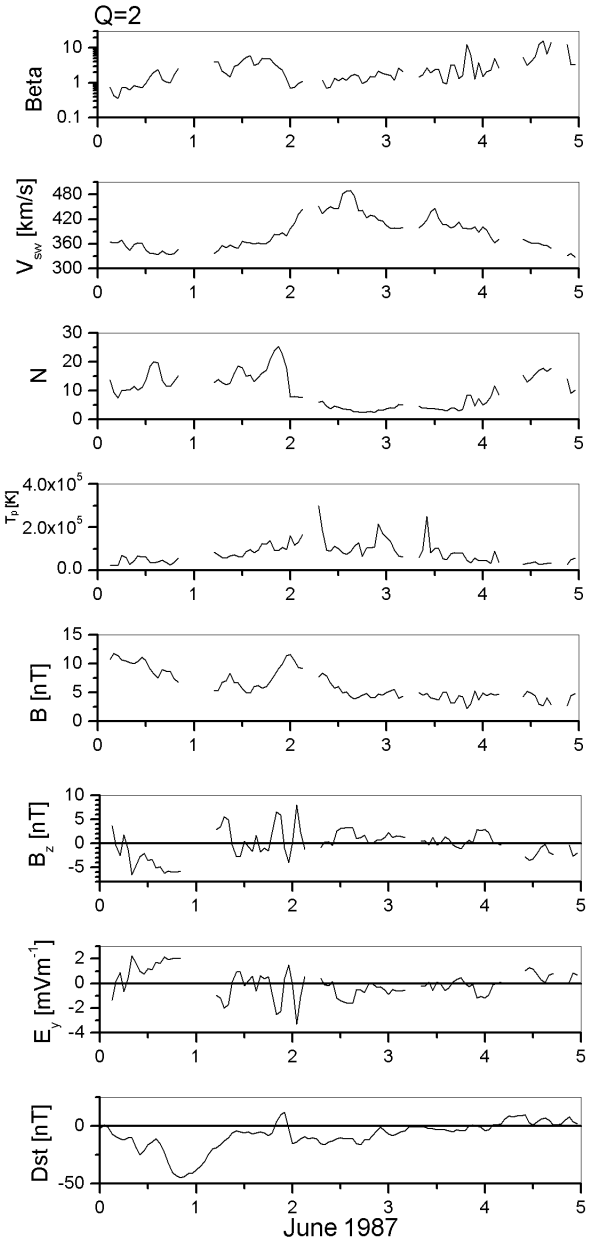

Figure 3. Example of event according quality of data, Q = 2. Plots are, from top to bottom, time variations of plasma parameters β, V_{sw}, n, T, B, B_s, E_y, and *Dst* index.

using WIND and ACE data. The hourly *Dst* index, for the studied period, was obtained from the World Data Center for Geomagnetism, Kyoto. For each one of the events, we found the Dst_p = minimum values of *Dst* index, the V_{max} = maximum value of V_{sw}, the B_p = maximum value of magnitude of B, the Bs_p = minimum value of south component of B, and the Ey_p = maximum value of Ey, all of them within until 2 days after the occurrence of the event.

3. Results of Statistical Analysis

[13] We have obtained, for the several parameters V_p, Bs_p, Ey_p, and Dst_p, the average value (AV), considering the total number of events for which we had the information available. Besides the AV in second column, Table 1 presents the standard deviation (SD), the minimum (Min) and the maximum (Max) observed values, the range (R) of parameter variation, i.e., the difference between Min and Max, and the number of events (N) we used. Table 1 also presents the variation coefficient (Cv = 100**AV*/*SD* (%)) and the median, i.e., the smallest value for each parameter such that at least half of the values in the distribution are no greater than it. Results from Table 1 indicate that intense or moderate magnetic storms do not usually follow CIRs.

[14] Once we have the minimum values of *Dst* index and of southward component of B, and the maximum values of V_{sw}, B, and E_y, within until 2 days after the data of each CIR event, we can obtain the distributions of percentage of CIRs against these parameters. Results are shown in Figures 5 and 6.

[15] Different explanations have been presented for the geomagnetic activity associated with CIRs. *Bobrov* [1973] suggested it was due to the highly fluctuating southward component of IMF. *Burlaga and Lepping* [1977] considered that the electric field, Ey, was the determinant parameter for geomagnetic activity. Since both V_{sw} and B_s determine the value of Ey, we present the distributions of percentage of CIRs against the maxima/minima of these parameters, together with the distribution for B_p. Figure 5a presents the distribution of percentage of CIRs against Bs_p. Concerning Bs_p, the distribution for CIRs and MCs (results from *Echer et al.* [2005b]) presents relevant differences. For CIRs, the maximum and the minimum values for Bs_p are 0 and −27 nT, respectively, while for MCs we have −2.4 nT and −31 nT. A difference is also noticed for the average value, −6.5 nT for CIRs and −10.5 nT for MCs. We can also observe a difference when comparing the value of median for Bs_p, −6.5 nT for CIRs, and −9.5 nT for MCs. Since B_s is an important parameter concerning geoeffectiveness, this result is an indication that CIRs are less geoeffective than MCs. Figure 5b shows the distribution of percentage of CIRs against B_p. The average value for B_p is 13.5 nT, with extremes 4.6 and 32 nT. It is interesting to observe that these results are very similar to the ones found when studying 149 MCs during the period 1966–2001, AV = 15.5 nT, Min = 5.2 nT, and Max = 37 nT [*Echer et al.*, 2005b]. Even the general behavior of the distribution is very similar, with a peak between 10 and 15 nT and decreasing for extreme values.

[16] The distribution of percentage of CIRs against the solar wind maximum speed, within until 2 days after the data of events, is shown in Figure 5c. The higher occurrence of CIRs is for velocities between 500 and 550 km/s, very close to the average value (∼600 km/s). As expected this AV is larger than the one found for MCs (485 km/s). The majority of the events has V_{max} between 400 and 800 km/s, while for MCs the majority of the events presents V_{max} between 350 and 550 km/s.

[17] As previously mentioned, the convection electric field ($Ey = V_{SW}B_s$) plays a determinant role on geomagnetic activity. A southward interplanetary field efficiently interconnects with the Earth's magnetic field, thereby mapping the solar wind electric field into the magnetosphere and ionosphere along the approximately equipotential interconnected field lines. Figure 5d presents the distribution of percentage of CIRs against Ey_p. The AV for Ey_p is

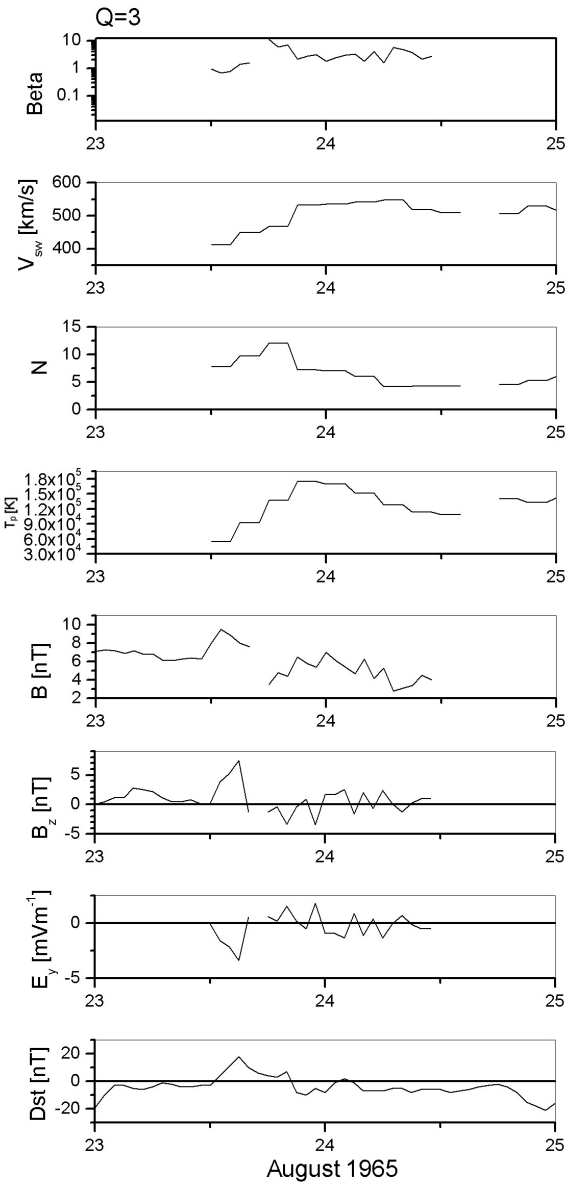

Figure 4. Example of event according quality of data, Q = 3. Plots are, from top to bottom, time variations of plasma parameters β, V_{sw}, n, T, B, B_s, E_y, and *Dst* index.

3.3 mV/m. Notice that this value is well below the criterion established by *Gonzalez and Tsurutani* [1987] as necessary to drive intense magnetic storms ($Dst \leq -100$ nT). Studying the interplanetary causes of intense magnetic storms, they found that Ey should be greater than 5 mV/m over a period exceeding 3 hours in order to cause intense magnetic storms. Although this limit has been established for a limited interval during solar maximum, it appears to hold also during solar minimum [*Tsurutani and Gonzalez*, 1995].

[18] Figure 6 shows the distribution of percentage of CIRs against the Dst_p for all CIR events. The majority of the CIR events presents Dst_p between −80 and −20 nT, relatively low as compared with MC results: between −150 and −30 nT [*Echer et al.*, 2005b]. The value of the median is a good representation for the different geoeffectiveness. For CIRs, the median of $Dst_p = -38$ nT, while for MCs is much higher, −81 nT. The average storm intensity associated with CIRs as quantified by Dst_p is around −43 nT, indicating on average weak geomagnetic activity. The AV of Dst_p is less than half of the value found for MCs (−94 nT), as expected, since several studies indicated that the most intense magnetic storms are related to ICMEs, MCs being, roughly, 1/3 of all ICMEs [*Gosling et al.*, 1990]. The distribution of percentage of MCs against the Dst_p, which values are mentioned here, can be found in Figure 2 of *Echer et al.* [2005b].

[19] In this paper we define geoeffectiveness as the percentage of the events that resulted in occurrence of magnetic storms of a certain class. In order to compare the results for CIRs with the ones obtained for other interplanetary structures such as shocks, magnetic clouds, and HCS sector boundary crossing, we use the same classification for geomagnetic activity used by *Echer et al.* [2005b] and *Echer and Gonzalez* [2004]. We consider four ranges of *Dst* index to indicate (1) quiet, $Dst > -30$ nT, (2) weak, -30 nT $\leq Dst < -50$ nT, (3) moderate, -50 nT $\leq Dst < -100$ nT, or (4) intense, $Dst \leq -100$ nT magnetic storm. Within CIRs, the B_s is typically highly fluctuating; the main phases of resultant magnetic storms have highly irregular profiles, in general, and are weaker than the ones that follow MCs [*Gonzalez et al.*, 1999]. Figure 7 presents a graph sector showing the percentage of CIRs that were followed by each type of geomagnetic activity conditions. It can be seen that less than 3% of CIRs are followed by intense geomagnetic storms. If we consider both types of activity, intense and moderate, ≈33% of CIRs are followed by geomagnetic activity, i.e., one third of CIRs are geoeffective.

[20] Since the beginning of the space age, the causes of geomagnetic activity have been sought in a number of correlative studies between solar wind parameters and various geomagnetic indices [e.g., *Snyder et al.*, 1963; *Gonzalez et al.*, 1998; *Badruddin*, 1998; *Wang et al.*, 2003; *Kane*, 2005]. Prior published studies have suggested that geomagnetic activity is related to changes in the interplanetary magnetic field (IMF) as well as to interplanetary plasma parameters. It is largely accepted that energy

Table 1. Statistics of CIR Parameters

Parameter	AV	SD	Median	Min	Max	Range	Cv	N
Dst_p, nT	−43.3	24.1	−38	−131	+9	140	56%	727
Ey_p, mV/m	3.3	1.6	3.0	−2.4	19.1	21.5	49%	613
B_p, nT	13.5	4.2	13.0	4.6	32.3	27.7	31%	658
Bs_p, nT	−7.0	3.1	−6.5	−27.3	0	27.3	44%	622
V_{max}, km/s	596	108	587	397	1194	797	18%	727

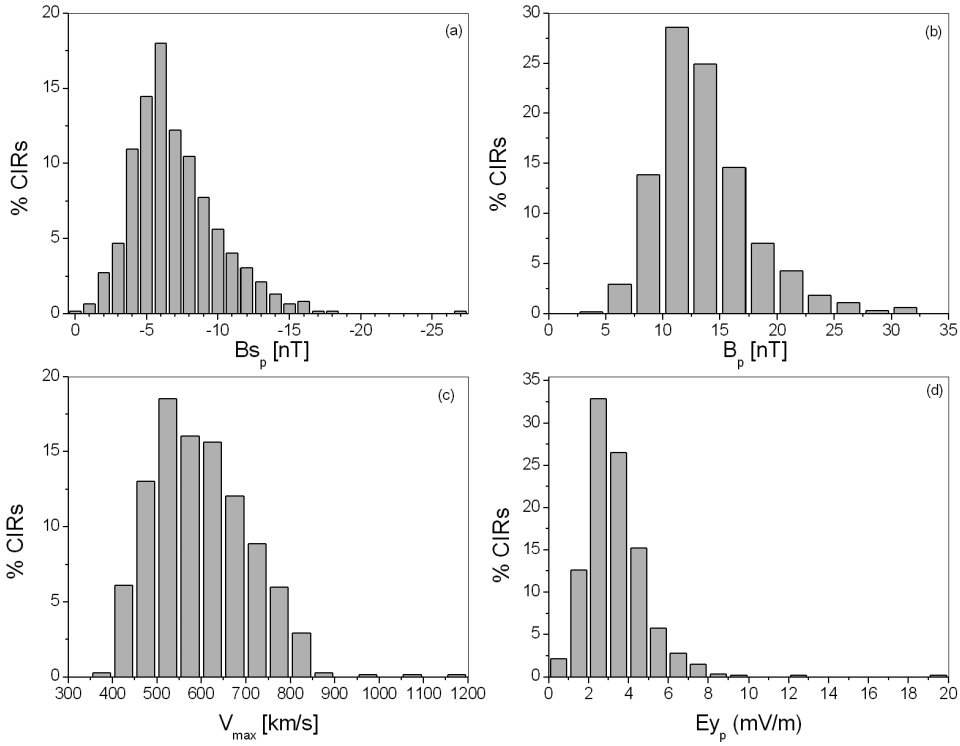

Figure 5. Distribution of percentage of CIRs against the peak values of (a) B_s, (b) B, (c) V_{sw}, and (d) Ey.

and particles can enter the magnetosphere when reconnection between the IMF and the geomagnetic field occurs. The penetration of these particles changes the intensity of the ring current leading to a reduction in the geomagnetic field, manifested by the variations on the *Dst* index. Here we look for some relation between the plasma parameters V_{max}, B_p, Bs_p, and the Dst_p for the CIR events.

[21] The B_s component is reported to be an important parameter for geomagnetic disturbances [*Gonzalez et al.*, 1994; *Tsurutani and Gonzalez*, 1995, and references therein]. Figure 8a shows the scatterplot of Dst_p versus Bs_p along with the linear fitting curve. The linear relation we obtain is $Dst_p = 10.1 + 4.7\ Bs_p$, with $r \approx 0.6$. For the magnitude of B, correlation is poor, $r \approx 0.33$, as shown in Figure 8b.

[22] Another parameter that appears as relevant for geomagnetic disturbances is V_{sw}. Figure 8c shows the scatterplot of Dst_p versus V_{max} along with the best linear fitting curve for the data. We observe that $r \approx 0.3$, indicating a poor relation between V_{max} and Dst_p. Similar results have been recently discussed by *Kane* [2005].

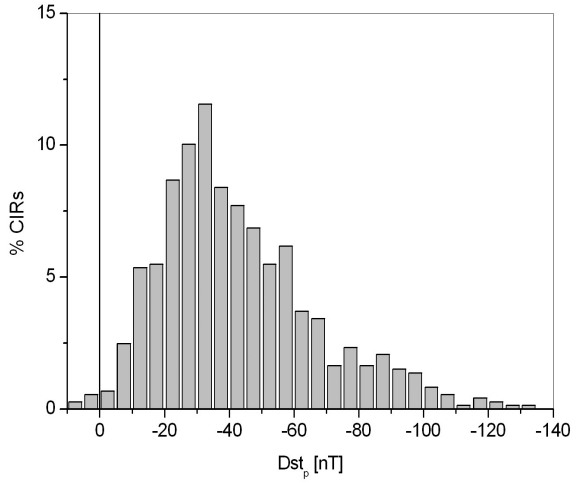

Figure 6. Distribution of percentage of CIRs against the minimum values of *Dst*.

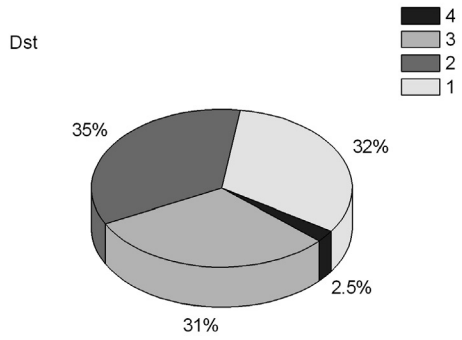

Figure 7. Graph sector showing the percentage of CIRs followed by each type of geomagnetic activity in terms of *Dst*.

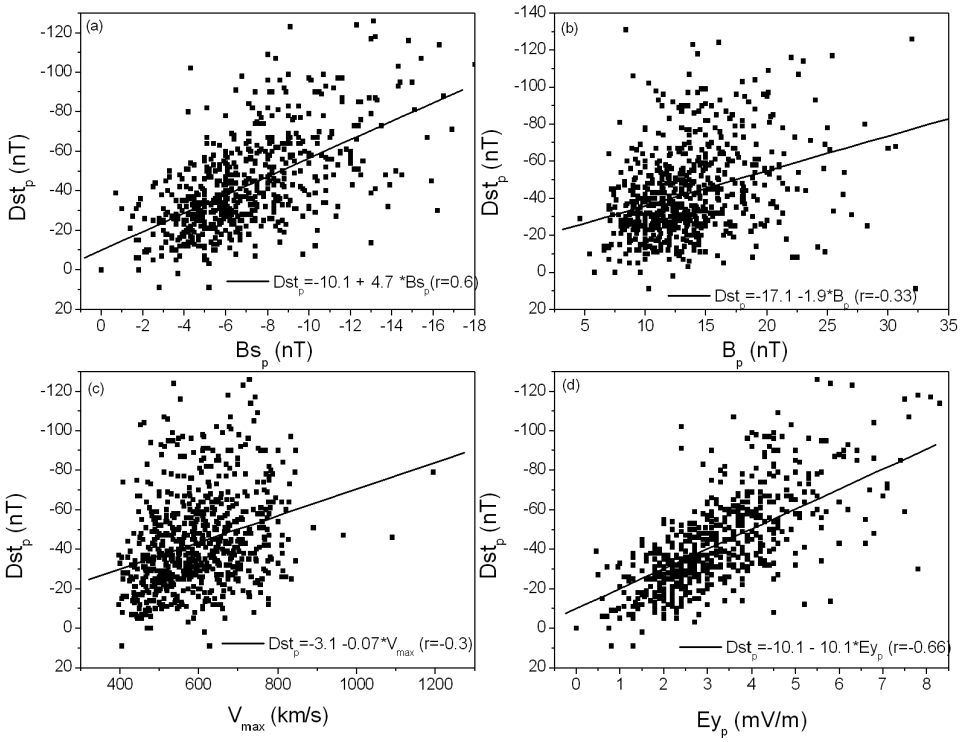

Figure 8. Scatterplots of solar wind parameters and geomagnetic index *Dst*. (a) Bs_p, (b) B_p, (c) V_{max} and (d) Ey_p, along with the linear fitting to the data.

[23] For reconnection theories, the main parameter is the product of solar wind velocity and Bs. Figure 8d shows the scatter plot for Ey_p versus Dst_p along with the linear fitting curve for the data. In that case we obtain the best correlation in this study, $r \approx 0.66$. This best correlation for Ey_p is expected, since the variation of *Dst* is well described by Burton's equation [see, e.g., *O'Brien and McPherron*, 2000]. It is important to mention that the correlation between Ey_p and Dst_p (0.66) is very close to the correlation between Dst_p and Bs_p (0.6), reflecting the fact that the variation of Ey is basically determined by Bs; the correlation between Dst_p and V_{max} is much smaller (0.3).

[24] It has been demonstrated by *Crooker and Cliver* [1994] that the Russell-McPherron effect exerts strong control over recurrent activity. In order to verify that, we performed analyses considering only the number of CIR events during equinox periods, September–October and March–April, and during solstice periods, November–February and May–August. For the equinox periods we found 114 and 113 CIRs, and for the solstice periods we found 242 and 241 events. For these separate data we obtained the same parameters we have obtained before. Although for all the other parameters the results are basically the same, the AV for the Dst_p increases to −51.7 nT for the period September–October and to −50 nT for the period March–April, both slightly higher when compared to −43 nT obtained when considering all events but still smaller then the one found for MCs, −94 nT. For the solstice periods, November–February and May–August, the AV values for Dst_p are −40 and −39 nT, respectively, very close to the one found when considering all events. During equinox periods, September–October and March–April, we found that 50% and 45%, respectively, of CIRs are geoeffective considering intense and moderate magnetic storms, larger then the 33% found when considering all events. For the solstice periods, less than 30% of CIRs are geoeffective, using the same criterion.

4. Conclusions

[25] In this paper we have analyzed the geoeffectiveness of CIRs during the solar wind observational period 1964–2003. We started by identifying the CIR events and looking for the level of geomagnetic activity that followed each CIR event. We obtained the distribution for maximum/minimum values of the interplanetary field and plasma parameters and *Dst*. Although the general behavior of these distributions is very similar to the ones obtained for the MCs, the maximum and minimum values we found for the plasma parameters within CIRs and MCs are very different. In particular, for the main parameters related to geoeffectiveness, the extremes are very different. While for CIRs, the maximum and the minimum values for Bs_p are 0 and −27 nT, respectively, for MCs we have −2.4 nT, and −31nT. A difference is also noticed for the average value, −6.5 nT for CIRs and −10.5 nT for MCs, and for the median values, −6.5 nT for CIRs and −9.5 nT for MCs. The median values for Dst_p are also very different, −38 nT for CIRs and −81 nT for MCs. The AV we found for Ey_p within CIR events is 3.3 mV/m. Notice that this value is well below the criterion established by *Gonzalez and Tsurutani* [1987] as necessary to drive intense magnetic storms. Since B_s and Ey are strongly related to magnetic activity, our results are an indication that CIRs are less geoeffective than MCs.

Yermolaev and Yermolaev [2002] looking for interplanetary disturbances that preceded magnetic storm with $Dst \leq -60$ nT, during 1976–2000, found the following: the interplanetary sources of magnetic storms are MCs in 33.2% of the events, CIRs in 30.2%, interplanetary shocks in 5.7%, and other solar wind structures in 30.9% of the events. When looking for only intense storms, i.e., $Dst \leq -100$ nT, the fraction of MCs associated with the events increases to one-half.

[26] Looking for the correlation between the maximum values of interplanetary field/plasma parameters and *Dst*, we found that the best correlations are for Bs_p or Ey_p ($r \geq 0.6$). Correlation between Dst_p with B_p or V_{max} is poor ($r \leq 0.33$), as expected and recently discussed by *Kane* [2005].

[27] Results of CIR geoeffectiveness can be compared with other isolated magnetic solar wind structures. *Echer and Gonzalez* [2004] have found the percentage of each one that is followed by intense and moderate storms: 57% of interplanetary shocks, 26% of sector boundary crossings (SBCs) of the heliospheric current sheet, and 77% of the magnetic clouds. These results can be contrasted with CIR events which presented ≈33% of them being geoeffective, i.e., followed by intense and moderate storms. This picture changes if we consider the CIR events occurring during equinox periods; in that case we found that approximately 50% of CIRs are followed by intense and moderate storms, reflecting the Russell-McPherron effect. Thus, in general, CIRs are less geoeffective than transient disturbances (shocks and MCs), but they are followed by a higher number of intense or moderate storms than simply the SBCs. *McAllister and Crooker* [1997] found evidences that a large storm would not occur after a SBC in the absence of a high-speed stream. The fact that CIRs are less geoeffective than transient disturbances is compatible with the fact that higher magnetic field strengths and consequently also large values of B_s and Ey, can be reached in transient disturbances, while within CIRs, IMF present a highly fluctuating southward component and small B_s enhancements.

[28] As pointed out by *Pizzo* [1982], the nonradial flow are driven by the total pressure gradients, so the approximate orientation of the interaction front relative to the equatorial plane can be inferred from the systematic variation of the flow direction across the leading edge of the stream. At least for some observational epoch, data on north-south as well as east-west flow deflections across stream fronts are available. The orientation of the stream front should be related to the magnitude of B_s generated by the CIR. An analysis of the north-south as well as east-west flow deflections across stream fronts is left for a future work.

[29] **Acknowledgments.** We thanks the ACE SWEPAM and MAG teams for making their data publicly available and the NSSDC at Goddard Space Flight Center for providing the OMNIWeb database. Thanks to National Geophysical Data Center and to the World Data Center for Geomagnetism for the *Dst* geomagnetic indices. This study was partially supported by research fellowship from CNPq (303343/2004-4). We also thank to the Brazilian agencies CAPES and FAPESP for financial support to attend the Chapman Conference. The authors would like to thank one of the reviewers for his valuable comments.

[30] Shadia Rifai Habbal thanks Victor Pizzo and another referee for their assistance in evaluating this paper.

References

Badruddin (1998), Interplanetary shocks, magnetic clouds, stream interfaces and resulting geomagnetic disturbances, *Planet. Space Sci.*, *46*, 1015–1028.

Bobrov, M. S. (1973), K_p index correlations with solar-wind parameters during the first and second stages of a recurrent geomagnetic storm, *Planet. Space Sci.*, *21*, 2139–2147.

Burlaga, L. F., and R. P. Lepping (1977), The cause of recurrent geomagnetic storms, *Planet. Space Sci.*, *25*, 1151–1160.

Burlaga, L. F., K. W. Behannon, S. F. Hansen, G. W. Pneumann, and W. C. Feldman (1978), Sources of magnetic fields in recurrent interplanetary streams, *J. Geophys. Res.*, *83*, 4177–4185.

Cane, H. V., and I. G. Richardson (2003), Interplanetary coronal mass ejections in the near-Earth solar wind during 1996–2002, *J. Geophys. Res.*, *108*(A4), 1156, doi:10.1029/2002JA009817.

Crooker, N. U., and E. W. Cliver (1994), Postmodern view of M-regions, *J. Geophys. Res.*, *99*, 23,383–23,390.

Dungey, J. W. (1961), Interplanetary magnetic field and the auroral zones, *Phys. Rev. Lett.*, *6*, 47–48.

Echer, E., and W. D. Gonzalez (2004), Geoeffectiveness of interplanetary shocks, magnetic clouds, sector boundary crossings and their combined occurrence, *Geophys. Res. Lett.*, *31*, L09808, doi:10.1029/2003GL019199.

Echer, E., W. D. Gonzalez, B. T. Tsurutani, L. E. A. Vieira, M. V. Alves, and A. L. C. Gonzalez (2005a), On the preferential occurrence of interplanetary shocks in July and November: Causes (solar wind annual dependence) and consequences (intense magnetic storms), *J. Geophys. Res.*, *110*, A02101, doi:10.1029/2004JA010527.

Echer, E., M. V. Alves, and W. D. Gonzalez (2005b), A statistical study of magnetic cloud parameters and geoeffectiveness, *J. Atmos. Sol. Terr. Phys.*, *67*, 839–852.

Feynman, J., and X. Y. Gu (1986), Prediction of geomagnetic activity on timescales of one to ten years, *Rev. Geophys.*, *24*, 650–659.

Forsyth, R. J., and E. Marsch (1999), Solar origin and interplanetary evolution of stream interfaces, *Space Sci. Rev.*, *89*, 7–20.

Gonzalez, W. D., and B. T. Tsurutani (1987), Criteria of interplanetary parameters causing intense magnetic storms (Dst < −100 nT), *Planet. Space Sci.*, *35*, 1101–1109.

Gonzalez, W. D., J. A Joselyn, Y. Kamide, H. W. Kroehl, G. Rostoker, B. T. Tsurutani, and V. M. Vasyliunas (1994), What is a geomagnetic storm?, *J. Geophys. Res.*, *99*, 5771–5792.

Gonzalez, W. D., A. L. C. Gonzalez, A. Dal lago, B. T. Tsurutani, J. K. Arballo, G. S. Lakhina, B. Buti, and C. M. Ho (1998), Magnetic cloud field intensities and solar wind velocities, *Geophys. Res. Lett.*, *25*, 963–966.

Gonzalez, W. D., B. T. Tsurutani, and A. L. Clua de Gonzalez (1999), Interplanetary origin of geomagnetic storms, *Space Sci. Rev.*, *88*, 529–562.

Gosling, J. T., and V. J. Pizzo (1999), Formation and evolution of corotating interaction regions and their three dimensional structure, *Space Sci. Rev.*, *89*, 21–52.

Gosling, J. T., S. J. Bame, and D. J. McComas (1990), Coronal mass ejections and large geomagnetic storms, *Geophys. Res. Lett.*, *17*, 901–904.

Hargreaves, J. K. (1992), *The Solar-Terrestrial Environment, Cambridge Atmos. and Space Sci. Ser.*, Cambridge Univ. Press, New York.

Hundhausen, A. J. (1995), The solar wind, in *Introduction to Space Physics*, edited by M. G. Kivelson and C. T. Russell, pp. 91–128, Cambridge Univ. Press, New York.

Iucci, N., M. Parissi, M. Storini, G. Villoressi, and R. Landi (1979), High-speed solar-wind streams and galactic cosmic-ray modulation, *Nuovo Cimento C*, *2*, 421–438.

Jackson, B. V. (1997), Heliospheric observations of solar disturbances and their potential role in the origin of storms, in *Magnetic Storms, Geophys. Monogr. Ser.*, vol. 98, edited by B. T. Tsurutani et al., pp. 59–70, AGU, Washington, D. C.

Kamide, Y, et al. (1998), Current understanding of magnetic storms: Storm-substorm relationships, *J. Geophys. Res.*, *103*, 17,705–17,728.

Kane, R. P. (2005), How good is the relationship of solar and interplanetary plasma parameters with geomagnetic storms?, *J. Geophys. Res.*, *110*, A02213, doi:10.1029/2004JA010799.

Krieger, A. S., A. F. Timothy, and E. C. Roelof (1973), A coronal hole and its identification as the source of high velocity solar wind stream, *Solar Phys.*, *29*, 505–525.

Lindblad, B. A., and H. Lundstedt (1981), A catalogue of high-speed plasma streams in the solar wind, *Solar Phys.*, *74*, 197–206.

Lindblad, B. A., and H. Lundstedt (1983), A catalogue of high-speed plasma streams in the solar wind 1975–78, *Solar Phys.*, *88*, 377–382.

Lindblad, B. A., H. Lundstedt, and B. Larsson (1989), A third catalogue of high-speed plasma streams in the solar wind data for 1978–1982, *Solar Phys.*, *120*, 145–152.

Lindsay, G. M., C. T. Russel, and J. G. Luhmann (1995), Coronal mass ejection and stream interaction region characteristics and their potential geoeffectiveness, *J. Geophys. Res.*, *100*, 16,999–17,013.

Mavromichalaki, H., and A. Vassilaki (1998), Fast plasma streams recorded near the Earth during 1985–1996, *Solar Phys.*, *183*, 181–200.

Mavromichalaki, H., A. Vassilaki, and E. Marmatsouri (1988), Catalogue of high-speed solar-wind streams: Further evidence of their relationship to Ap index, *Solar Phys.*, *115*, 345–365.

McAllister, A. H., and N. U. Crooker (1997), Coronal mass ejections, corotating interaction regions, and geomagnetic storms, in *Coronal Mass Ejections*, *Geophys. Monogr. Ser.*, vol. 99, edited by N. Crooker et al., pp. 279–190, AGU, Washington, D. C.

O'Brien, T. P., and R. L. McPherron (2000), Forecasting the ring current index *Dst* in real time, *J. Atmos. Sol. Terr. Phys.*, *62*, 1295.

Phillips, J. L., A. Balogh, S. J. Bame, B. E. Goldstein, J. T. Gosling, J. T. Hoeksema, D. J. McComas, M. Neugebauer, N. R. Sheeley Jr., and Y. M. Yang (1994), Ulysses at 50° south: Constant immersion in the high-speed solar wind, *Geophys. Res. Lett.*, *21*, 1105.

Pizzo, V. (1978), A three-dimensional model of corotating streams in the solar wind: 1. Theoretical foundations, *J. Geophys. Res.*, *83*, 5563–5572.

Pizzo, V. (1982), A three-dimensional model of corotating streams in the solar wind: 3. Magnetohydrodynamic streams, *J. Geophys. Res.*, *87*, 4374–4394.

Richardson, I. G., E. W. Cliver, and H. V. Cane (2000), Sources of geomagnetic activity over the solar cycle: Relative importance of coronal mass ejections, high-speed streams, and slow solar wind, *J. Geophys. Res.*, *105*, 18,203–18,213.

Russell, C. T., and R. L. McPherron (1973), Semiannual variation of geomagnetic activity, *J. Geophys. Res.*, *78*, 92–108.

Sheeley, N. R., Jr., and J. W. Harvey (1981), Coronal holes, solar wind streams, and recurrent geomagnetic disturbances during 1978 and 1979, *Solar Phys.*, *70*, 237.

Smith, E. J., and J. H. Wolf (1976), Observations of interaction regions and corotating shocks between one and five AU Pioneers 10 and 11, *Geophys. Res. Lett.*, *3*, 137.

Snyder, C. W., M. Neugebauer, and U. R. Rao (1963), The solar wind velocity and its correlation with cosmic ray variations and with solar and geomagnetic activity, *J. Geophys. Res.*, *68*, 6361.

Timothy, A. F., A. S. Krieger, and G. S. Vaiana (1975), The structure and evolution of coronal holes, *Solar Phys.*, *42*, 135.

Tsurutani, B. T., and W. D. Gonzalez (1995), The future of geomagnetic storm predictions: implications from recent solar and interplanetary observations, *J. Atmos. Terr. Phys.*, *57*, 1369.

Tsurutani, B. T., M. E. Burton, E. J. Smith, and D. E. Jones (1987), Statistical properties of magnetic field fluctuations in the distant plasma sheet, *Planet. Space Sci.*, *35*, 289.

Tsurutani, B. T., W. D. Gonzalez, A. L. C. Gonzalez, F. Tang, J. K. Arballo, and M. Okada (1995), Interplanetary origin of geomagnetic activity in the declining phase of solar cycle, *J. Geophys. Res.*, *100*, 21,717–21,733.

Wang, Y., C. L. Shen, S. Wang, and P. Z. Ye (2003), An empirical formula relating the geomagnetic storm's intensity to the interplanetary parameters: $-VB_z$ (average) and Δt, *Geophys. Res. Lett.*, *30*(20), 2039, doi:10.1029/2003GL017901.

Yermolaev, Y. I., and M. Y. Yermolaev (2002), Statistical relationships between interplanetary and geomagnetic disturbances 1976–2000, *Cosmic Res.*, *40*, 1–14.

Yermolaev, Y. I., M. Y. Yermolaev, G. N. Zastenker, L. M. Zelenyi, A. A. Petrukovich, and J.-A. Sauvaud (2005), Statistical studies of geomagnetic storm dependencies on solar and interplanetary events: A review, *Planet. Space Sci.*, *53*, 189–196.

M. V. Alves, Laboratório Associado de Plasma, Instituto Nacional de Pesquisas Espaciais, MCT, Av. dos Astronautas 1758, 12227-010 São José dos Campos, São Paulo, Brazil. (virginia@plasma.inpe.br)

E. Echer and W. D. Gonzalez, Divisão de Geofisica Espacial, Instituto Nacional de Pesquisas Espaciais, MCT, Av. dos Astronautas 1758, 12227-010 São José dos Campos, São Paulo, Brazil.